J Sol-Gel Sci Technol (2010) 53:405–411
DOI 10.1007/s10971-009-2112-1

ORIGINAL PAPER

Synthesis and magnetic properties of nanocomposite $Ni_{1-x}Co_xFe_2O_4$–$BaTiO_3$ fibers by organic gel-thermal decomposition process

Xiangqian Shen · Zhi Zhou · Fuzhan Song · Xianfeng Meng

Received: 9 September 2009 / Accepted: 6 November 2009 / Published online: 1 December 2009

Abstract Nanocomposites of ferrite and ferroelectric phases are attractive functional ceramic materials. In this work, the nanocomposite $Ni_{1-x}Co_xFe_2O_4$–$BaTiO_3$($x = 0.2$, 0.3, 0.4, 0.5) fibers with fine diameters of 3 $\sim$ 7 μm and high aspect ratios were synthesized by the organic gel-thermal decomposition process from the raw materials of citric acid and metal salts. The structure, thermal decomposition process and morphologies of the gel precursors and the resultant fibers derived from thermal decomposition of the gel precursors were characterized by Fourier transform infrared spectroscopy, thermogravimetric differential thermal analysis, X-ray diffraction and scanning electron microscopy. The magnetic properties of the nanocomposite fibers were measured by vibrating sample magnetometer. The nanocomposite fibers of ferrite $Ni_{1-x}Co_xFe_2O_4$ and perovskite $BaTiO_3$ are formed at the calcination temperature of 900 °C for 2 h. The average grain sizes of $Ni_{1-x}Co_xFe_2O_4$ and $BaTiO_3$ in the nanocomposite fibers increase from about 15 nm to approximately 67 nm with the increasing calcination temperatures from 900 to 1,180 °C. The saturation magnetization of the nanocomposite $Ni_{1-x}Co_xFe_2O_4$–$BaTiO_3$($x = 0.2$, 0.3, 0.4, 0.5) fibers increases with the increase of grain sizes of $Ni_{1-x}Co_xFe_2O_4$ and Co content, while the coercivity reaches a maximum value at the single-domain size of about 65 nm of $Ni_{0.5}Co_{0.5}Fe_2O_4$ obtained at the calcination temperature of 1,100 °C.

Keywords Nanocomposite fibers · Organic gel-thermal decomposition process · Ferrite · Magnetic property

X. Shen (✉) · Z. Zhou · F. Song · X. Meng
School of Materials Science and Engineering, Jiangsu University, 212013 Zhenjiang, China
e-mail: shenxq@ujs.edu.cn

1 Introduction

Multiferroic magnetoelectric composite materials, which consist of ferromagnetic and ferroelectric phases and simultaneously exhibit magnetic and electric orderings, have stimulated a increasing number of research activities for their functional features and potential applications in advanced multifunctional devices such as magnetic sensors, microwave devices, transformers and actuators et al. [1–3]. The heterostructures of nanocomposite, solid solution and superlattice are allowed to acquire a tight coupling between the ferromagnetic and ferroelectric phases [4, 5]. Compared with multilayer structures, the nanocomposite multiferroic fibers consisting of ferrite and ferroelectric phases can produce a maximum intrinsic magnetoelectric coupling without the substrate constraint and can magnify the mechanical displacement arising from the piezoelectric or magnetostrictive effect due to a high aspect ratio [6, 7].

Quasi-one-dimensional (Q1D) nanostructured multiferroic materials are potential building blocks for the next-generation electromagnetic devices [8]. At present, there are two methods used for preparation of Q1D ferromagnetic and ferroelectric composite materials. Hua et al. [9] synthesized $CoFe_2O_4$/Pb $(Zr_{0.52}Ti_{0.48})O_3$(PZT) nanotubes by the sol–gel template process. These $CoFe_2O_4$/PZT composite nanotubes were characterized with diameters of 80 $\sim$ 300 nm, and about 100 μm in length. Xie et al. [10] prepared $CoFe_2O_4$/PZT nanofibers by electrospinning with diameters of 100 $\sim$ 300 nm. However, the template and electrospinning processes are considered hard to efficiently produce Q1D multiferroic materials on a large scale. There is therefore a demand for the preparative process of nanocomposite multiferroic fibers. Due to simple and low cost, the gel thermal decomposition process is commonly used to prepare single phase metal and ceramic fibers

[11, 12]. The aim of this investigation is to fabricate nanocomposite $Ni_{1-x}Co_xFe_2O_4$–$BaTiO_3$($x = 0.2, 0.3, 0.4, 0.5$) fibers by the organic gel-thermal decomposition process and examine the magnetic properties of these nanocomposite fibers.

2 Experimental

The nanocomposite $0.5Ni_{1-x}Co_xFe_2O_4$–$0.5BaTiO_3$($x = 0.2, 0.3, 0.4, 0.5$) fibers were prepared by the organic gel-thermal decomposition process and the process was described in detail previously [13]. The starting reagents used were analytical grade $Fe(NO_3)_3{\cdot}9H_2O$, $NiCO_3{\cdot}2Ni(OH)_2{\cdot}4H_2O$, $Co(NO_3)_2{\cdot}6H_2O$, $BaCO_3$, $Ti(OC_4H_9)$ and citric acid. The required metal salts and citric acid were dissolved in an aqueous and ethanol hybrid solution at pH 7.0 with a continuous magnetic stirring. The solution was magnetically stirred for 20 ~ 24 h at room temperatures and then removed surplus water in a vacuum rotary evaporator at 60 ~ 80 °C until a viscous liquid was obtained. The gel fibers were drawn from the spinnable gels by the domestic machine and dried in a vacuum oven at 80 °C for about 24 h. The dried gel fibers were then put in an alumina crucible and subsequently were calcined at different temperatures for 2 h under an ambient atmosphere to form the nanocomposite fibers.

The structure, composition and morphologies of the gel precursors and the resultant fibers were examined by Fourier transform infrared spectroscopy (FTIR) using a model of Nexu670 spectrometer, X-ray diffraction (XRD) using a D/max2500PC diffractometer (RIGAKU), and scanning electron microscopy (SEM) using a field emission scanning electron microscopy (JSM-7001F). The decomposition process was investigated by thermo-gravimetric (TG) analysis and differential scanning calorimetry (DSC) using a SDT2960 (TA) system. Magnetic measurements were carried out at room temperatures by a vibrating sample magnetometer (VSM).

3 Results and discussion

3.1 FTIR spectra of gel precursor and fibers calcined at different temperatures

Figure 1 shows the FTIR spectra of the gel precursor for $0.5Ni_{0.5}Co_{0.5}Fe_2O_4$–$0.5BaTiO_3$ fibers and the products derived from calcination of the precursor at different temperatures. From the FTIR spectrum for the gel precursor in Fig. 1a, the two bands at 1,614 and 1,384 cm^{-1} arise from the $RCOO^-$ symmetrical and asymmetrical stretching vibration, which are the characteristic absorption

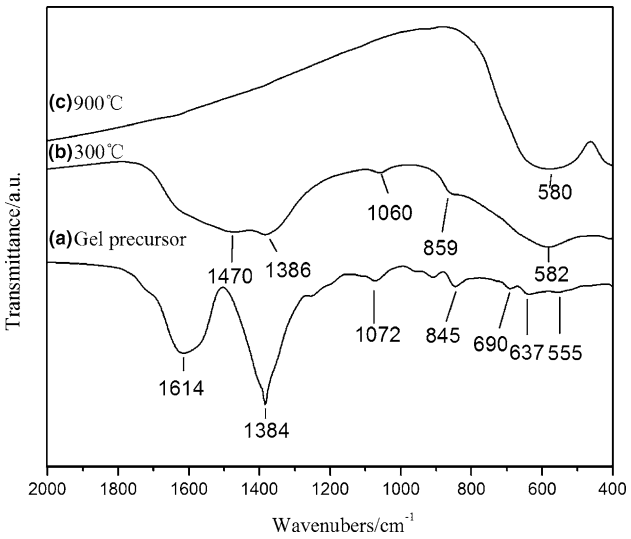

Fig. 1 FTIR spectra of the gel precursor and composite fibers calcined at different temperatures

peaks for the citrate. The bands at 1,072, 845, 690, 637 and 555 cm^{-1} can be assigned to the characteristic vibration peaks of C–OH, Ti–O, Co–O, Ni–O and Fe–O bonds [14–16], respectively. This is indicative of the complex formation of metal ions and citric acid.

For the samples obtained at 300 °C, as shown in Fig. 1b, the characteristic absorption peak for the citrate at around 1,614 cm^{-1} disappears owing to the decomposition of citrate. Two bands at 1,470 and 859 cm^{-1} can be assigned to the characteristic absorption peaks for $BaCO_3$. The bands at 1,386 and 1,060 cm^{-1} are corresponding the characteristic vibration peaks of NO_3^- and Fe_2O_3, and the band at about 582 cm^{-1} is assigned to NiO_2, Co_3O_4 and TiO_2 [17–19]. With the calcination temperature increased to 900 °C, as shown in Fig. 1c, the peaks assigned to $BaCO_3$ and metal oxides disappear and the characteristic peak at around 580 cm^{-1} is detected due to the stretching mode of Fe–O at tetrahedral sites in the spinel structure and the stretching mode of Ti–O in the perovskite $BaTiO_3$, which indicates that $Ni_{0.5}Co_{0.5}Fe_2O_4$ and $BaTiO_3$ would be formed at this calcination temperature [20, 21].

3.2 Thermal decomposition of gel precursor

Figure 2 shows the TG-DSC curves of the $0.5Ni_{0.5}Co_{0.5}Fe_2O_4$–$0.5BaTiO_3$ gel precursor and the thermal decomposition process roughly consists of the following three stages. The first stage takes place at the temperature range of 50 ~ 300 °C. The DSC curve exhibits a broad endothermic event corresponding to a weight loss of about 10% at low temperatures 50 ~ 180 °C and this is attributed to the loss of free water and bound water from the gel precursor. Then a large and sharp exothermic event occurs at

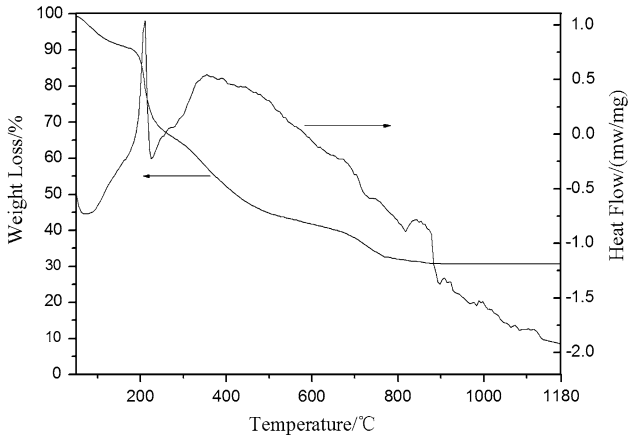

Fig. 2 TG/DSC curves of gel precursor for $0.5Ni_{0.5}Co_{0.5}Fe_2O_4$–$0.5BaTiO_3$ fibers

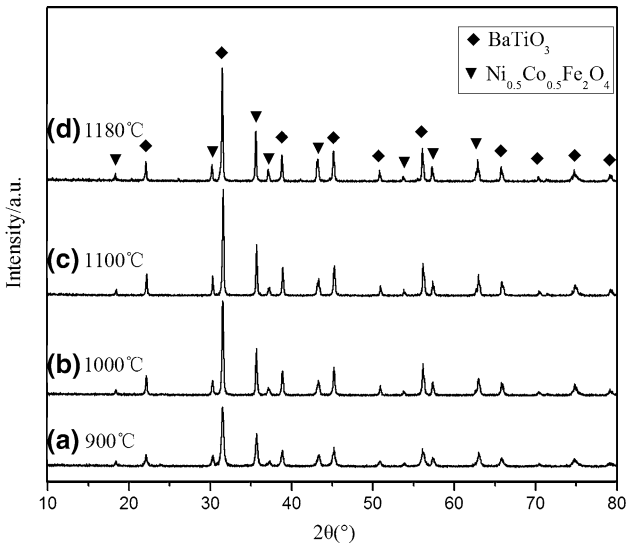

Fig. 3 XRD patterns of nanocomposite $0.5Ni_{0.5}Co_{0.5}Fe_2O_4$–$0.5BaTiO_3$ fibers calcined at different temperatures

around 210 °C in the DSC curve correspondingly a weight loss of about 27%, owing to the initial break-down of the complexes and a spontaneous combustion. The spontaneous combustion is induced by the in situ oxidizing interactions of citrate, nitrate ions and ammonium nitrate in the gel accompanying with liberation of H_2O, CO_2, NO_X [22, 23].

The second stage at the temperature range of 300 ~ 900 °C, the DSC curve exhibits a broad exothermic event and a series of small endothermic peaks. The broad exothermic event at around 380 °C is accompanied by a weight loss of 23% due to continuing oxidation of the organic matters and formation of metal oxides. A series of small endothermic peaks at around 800 °C correspond to a weight loss of about 10%, and it is believed that at this temperature range the formation of $Ni_{0.5}Co_{0.5}Fe_2O_4$ and $BaTiO_3$ takes place.

The third stage at the temperature range of 900 ~ 1,180 °C, the TG curve shows almost no changes in weight loss and some small endothermic events occur in the DSC curve owing to the crystallization and grain growth of the formed $Ni_{0.5}Co_{0.5}Fe_2O_4$ and $BaTiO_3$, which is evidenced by the above FTIR (Fig. 1c) analysis and confirmed by the following XRD data.

3.3 Structural characterization of nanocomposite $0.5Ni_{1-x}Co_xFe_2O_4$–$0.5BaTiO_3$ fibers

Figure 3 shows XRD patterns of the nanocomposite $0.5Ni_{0.5}Co_{0.5}Fe_2O_4$–$0.5BaTiO_3$ fibers obtained at various calcination temperatures for 2 h. After calcination at 900 °C, the diffraction collections are indexed just to both the spinel ferrite $NiFe_2O_4$ (JCPDS No. 10-0325) and perovskite $BaTiO_3$ (JCPDS No. 05-0626) phases, which is in agreement with the above FTIR and TG/DSC analyses. As the ferrite $NiFe_2O_4$ has the same structure with $Ni_{0.5}Co_{0.5}Fe_2O_4$, it can be deduced that the composite consisting of the ferrite $Ni_{0.5}Co_{0.5}Fe_2O_4$ and perovskite $BaTiO_3$ is formed at this calcination temperature. With the calcination temperature increasing from 900 to 1,180 °C, the corresponding peaks become sharper and narrower, and the crystallization of $Ni_{0.5}Co_{0.5}Fe_2O_4$ and $BaTiO_3$ is improved and the consequent crystalline grains grow.

The average crystalline size (D) of $Ni_{1-x}Co_xFe_2O_4$ and $BaTiO_3$ phases in the fibers can be calculated from the full width at half maximum (FWHM) of the reflection peaks of (311) and (101) using Scherrer's equation. The calculated average crystalline grain size D of $Ni_{1-x}Co_xFe_2O_4$ and $BaTiO_3$ phases in $0.5Ni_{1-x}Co_xFe_2O_4$–$0.5BaTiO_3$($x = 0.2$, 0.3, 0.4, 0.5) fibers with the calcination temperatures is plotted in Fig. 4. The crystalline grain sizes are influenced largely by the calcination temperature and the cobalt content in $Ni_{1-x}Co_xFe_2O_4$. For both $Ni_{1-x}Co_xFe_2O_4$ and $BaTiO_3$ phases at low cobalt content 0.2, D values increase from about 15 to 55 nm with the calcination temperature from 900 to 1,180 °C. By substitution of Ni with Co in $Ni_{1-x}Co_xFe_2O_4$, the grain sizes of $Ni_{1-x}Co_xFe_2O_4$ and $BaTiO_3$ tend to increase at various calcination temperatures, whilst it finds that the average grain size of $BaTiO_3$ in $0.5Ni_{0.5}Co_{0.5}Fe_2O_4$–$0.5BaTiO_3$ composite has almost a same size when the calcination temperature over 1,000 °C.

The lattice parameter of $Ni_{1-x}Co_xFe_2O_4$ was calculated by use of a special software (MDI Jade 5.0). The average grain size and lattice parameter of $Ni_{1-x}Co_xFe_2O_4$ with various Co content obtained at 1,180 °C are represented in Table 1. It can be seen that from Table 1 that the grain size and lattice parameter of $Ni_{1-x}Co_xFe_2O_4$ increase with Co content, owing to the crystal lattice inflation induced by the substitution of Ni cations (0.78 Å) with larger Co cations

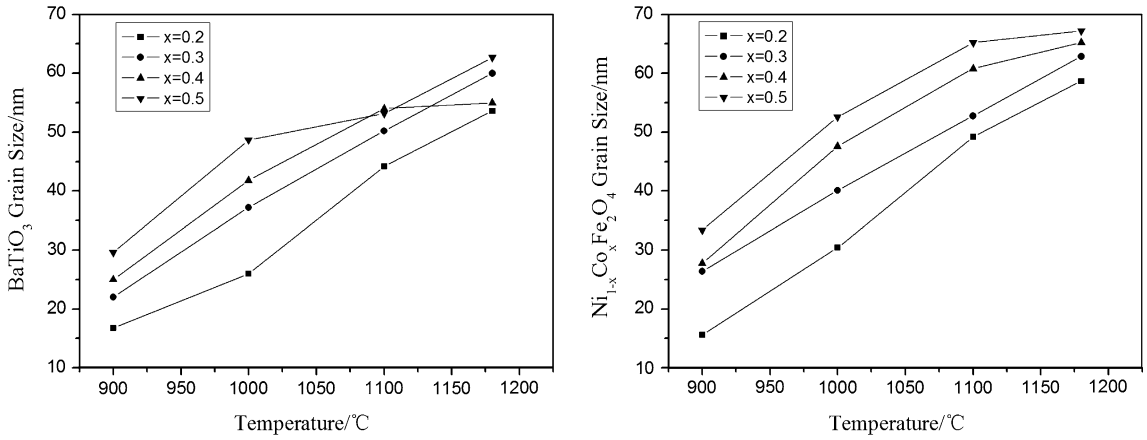

Fig. 4 Grain sizes of $Ni_{1-x}Co_xFe_2O_4$($x = 0.2, 0.3, 0.4, 0.5$) and $BaTiO_3$ in nanocomposite $0.5Ni_{1-x}Co_xFe_2O_4$–$0.5BaTiO_3$ fibers with calcination temperature

(0.82 Å) [24]. The grain sizes and the coupling of ferromagnetic $Ni_{1-x}Co_xFe_2O_4$ and ferroelectric $BaTiO_3$ nanophases so that can be tailored by controlling the calcination process and chemical composition.

The SEM graphs of the typical nanocomposite $0.5Ni_{0.5}Co_{0.5}Fe_2O_4$–$0.5BaTiO_3$ fibers obtained at 1,180 °C for 2 h are showed in Fig. 5. It can be seen that the fibers are characterized with a diameter range of $3 \sim 7$ μm, a high aspect ratio up to 1×10^3 and a dense surface. These fibers are composed of nanosized particles of $Ni_{0.5}Co_{0.5}Fe_2O_4$ and $BaTiO_3$. In comparison with the average crystalline size estimated by Scherrer's equation, the particle size observed is in a range 50 to 300 nm and generally in a nano-scale, whilst some particles are larger possibly owing to particle aggregations. The morphologies of the other nanocomposite $0.5Ni_{1-x}Co_xFe_2O_4$–$0.5BaTiO_3$($x = 0.2, 0.3, 0.4, 0.5$) fibers are very similar.

3.4 Magnetic properties

The hysteresis loops were measured to determine saturation magnetization (M_s) and coercivity (H_c). Figure 6 shows the hysteresis loops of the randomly oriented nanocomposite $0.5Ni_{0.5}Co_{0.5}Fe_2O_4$–$0.5BaTiO_3$ fibers obtained at different calcination temperatures for 2 h. These loops are characterized with typical soft magnetic properties of

Table 1 The effects of Co content (x) on grain size (D) and lattice parameter (a) of $Ni_{1-x}Co_xFe_2O_4$ and M_s and H_c of $0.5Ni_{1-x}Co_xFe_2O_4$–$0.5BaTiO_3$ fibers obtained at 1,180 °C

Co (x)	D (nm)	a (Å)	M_s (Am^2kg^{-1})	H_c (kAm^{-1})
0.2	58.7	8.345	12.95	26.32
0.3	62.9	8.347	14.98	27.80
0.4	65.2	8.355	15.79	27.52
0.5	67.4	8.366	20.62	24.73

$Ni_{0.5}Co_{0.5}Fe_2O_4$ ferrite, implying a magnetic ordering in the as-prepared nanocomposite fibers. The magnetic parameters of the $Ni_{0.5}Co_{0.5}Fe_2O_4$–$BaTiO_3$ fibers with calcination temperature are represented in Table 2. It can be seen that M_s and magnetic remance (M_r) increase from 7.69 to 20.62 Am^2/kg and 0.70 to 7.05 Am^2/kg, respectively corresponding the calcination temperature from 900 to 1,180 °C. This phenomenon can be explained due to the crystallization improvement and grain growth of the ferrite [25].

As showed in Table 2, the coercivity increases initially with the calcination temperature and reaches a maximum value at around 1,100 °C due to the increasing magnetocrystalline anisotropy. According to the Stoner–Wohlfarth single-domain theory [26], when the crystalline grain size of $Ni_{0.5}Co_{0.5}Fe_2O_4$ is within the single-domain size, the magnetocrystalline anisotropy energy of a nanocrystal single domain $Ni_{0.5}Co_{0.5}Fe_2O_4$ is proportion to the volume of nanocrystal particles and the magnetocrystalline anisotropy of $Ni_{0.5}Co_{0.5}Fe_2O_4$ increases with the increasing grain size from about 34 to 65 nm corresponding the calcination temperature from 900 to 1,100 °C as showed in Table 2. With a further increase of calcination temperature over 1,100 °C, the coercivity then exhibits a reduction tendency as the $Ni_{0.5}Co_{0.5}Fe_2O_4$ grain size is larger than the single-domain size and the particles become multi-domains. The domain-wall motions taking place in these multi-domain particles will result in the coercivity reduction [27]. It can be reasoned that the single-domain size of $Ni_{0.5}Co_{0.5}Fe_2O_4$ in the nanocomposite $Ni_{0.5}Co_{0.5}Fe_2O_4$–$BaTiO_3$ fibers is around 65 nm, which is close to the value 70 nm for $CoFe_2O_4$ particles reported by Rashada et al. [28] and 100 nm for $NiFe_2O_4$ particles reported by Yao et al. [29]. The effect of calcination temperature on the squareness (M_r/M_s) of $Ni_{0.5}Co_{0.5}Fe_2O_4$ in the nanocomposite fibers is similar to that of coercivity.

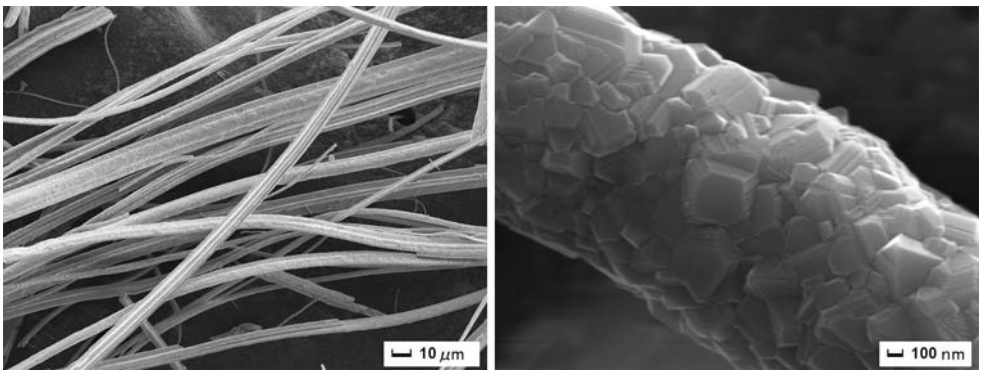

Fig. 5 SEM morphologies of $0.5Ni_{0.5}Co_{0.5}Fe_2O_4$–$0.5BaTiO_3$ fibers obtained at 1,180 °C for 2 h

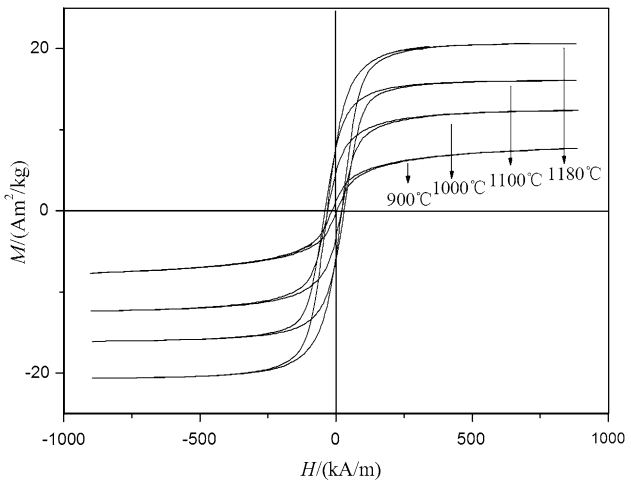

Fig. 6 Hysteresis loops of randomly oriented nanocomposite $0.5Ni_{0.5}Co_{0.5}Fe_2O_4$–$0.5BaTiO_3$ fibers obtained at different calcination temperatures

Figure 7 shows the hysteresis loops of the randomly oriented nanocomposite $0.5Ni_{1-x}Co_xFe_2O_4$–$0.5BaTiO_3$ ($x = 0.2, 0.3, 0.4, 0.5$) fibers obtained at 1,180 °C for 2 h. The saturation magnetization of $Ni_{1-x}Co_xFe_2O_4$–$BaTiO_3$($x = 0.2, 0.3, 0.4, 0.5$) fibers obtained at 1,180 °C for 2 h are represented in Table 1. It can be seen that M_s vaules increase from 12.95 to 20.62 Am^2/kg with the increase of Co content, which is mainly due to the substitution of Ni^{2+}ions by Co^{2+} ions in the octahedral sites and higher magnetic moment of Co^{2+} ions [30]. In order to compare the magnetic properties, the hysteresis loops of $CoFe_2O_4$ and $NiFe_2O_4$ fibers calcined at 1,180 °C are also showed in Fig. 7. Compared with the saturation magnetization of the single phase $CoFe_2O_4$ fibers (87.77 Am^2/kg) and $NiFe_2O_4$ fibers (24.85 Am^2/kg), the $0.5Ni_{1-x}Co_xFe_2O_4$–$0.5BaTiO_3$ ($x = 0.2, 0.3, 0.4, 0.5$) nanocomposite fibers exhibit lower M_s values owing to non-magnetic $BaTiO_3$ phase. The H_c values for these nanocomposite fibers are distributed between the coercivity value of $CoFe_2O_4$ fibers (52.42 kA/m) and $NiFe_2O_4$ fibers (6.65 kA/m), implying the magnetization behaviour and magnetic ordering for the nanocomposite fibers can be tailored by design of the chemical composition.

4 Conclusions

(1) The nanocomposite $0.5Ni_{1-x}Co_xFe_2O_4$–$0.5BaTiO_3$($x = 0.2, 0.3, 0.4, 0.5$) fibers have been successfully prepared by the organic gel-thermal decomposition process using citric acid and metal salts as the starting reagents. These fibers are composed of nanosized ferrite $Ni_{1-x}Co_xFe_2O_4$ and perovskite $BaTiO_3$ and have a diameter range from 3 to 7 μm, a high aspect ratio and a dense surface.

(2) The average grain sizes of $Ni_{1-x}Co_xFe_2O_4$ and $BaTiO_3$ in the nanocomposite fibers increase from about 15 to 67 nm, 17 to 64 nm with the calcination temperature from 900 to 1,180 °C, respectively. The grain size and lattice parameter of $Ni_{1-x}Co_xFe_2O_4$ increase in the cobalt content range of 0.2 to 0.5 at various calcination temperatures.

Table 2 Effects of calcination temperature on $Ni_{0.5}Co_{0.5}Fe_2O_4$ grain size (D) and magnetic properties of nanocomposite $0.5Ni_{0.5}Co_{0.5}Fe_2O_4$–$0.5BaTiO_3$ fibers

Temperature (°C)	D (nm)	M_s (Am^2kg^{-1})	M_r (Am^2kg^{-1})	M_r/M_s	H_c (kAm^{-1})
900	33.4	7.69	0.70	0.09	8.78
1,000	52.6	12.37	3.96	0.29	26.05
1,100	65.2	16.10	6.63	0.41	33.72
1,180	67.2	20.62	7.05	0.34	24.73

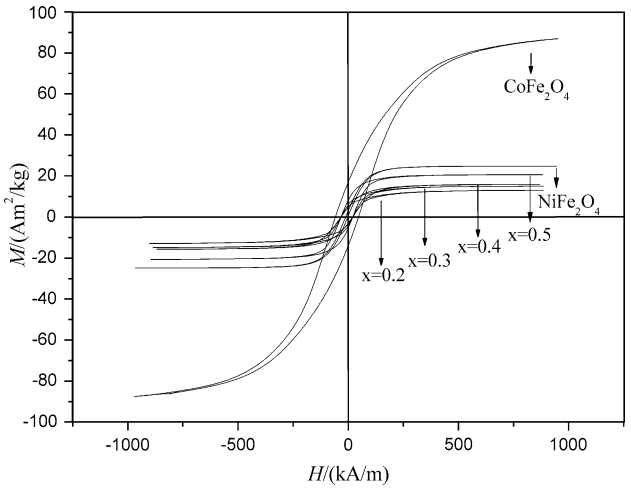

Fig. 7 Hysteresis loops of randomly oriented $0.5Ni_{1-x}Co_xFe_2O_4$-$0.5BaTiO_3$($x = 0.2, 0.3, 0.4, 0.5$) fibers,$CoFe_2O_4$ and $NiFe_2O_4$ fibers obtained at 1,180 °C for 2 h

(3) The magnetic properties for the nanocomposite fibers are largely influenced by the grain size of $Ni_{1-x}Co_xFe_2O_4$ and Co content. The saturation magnetization of $0.5Ni_{1-x}Co_xFe_2O_4$–$0.5BaTiO_3$ fibers increases with the grain size and cobalt content, whilst the coercivity reaches a maximum value at the single-domain size of about 65 nm of $Ni_{0.5}Co_{0.5}Fe_2O_4$ obtained at the calcination temperature of 1,100 °C.

Acknowledgments This work was supported by the National Natural Science Foundation of China (Grant No. 50674048, 50474038) and China Postdoctoral Science Foundation (Grant No. 20080431069).

References

1. Dong SX, Li JF, Viehland D (2004) Voltage gain effect in a ring-type magnetoelectric laminate. Appl Phys Lett 84:4188–4191
2. Semenov AA, Karmanenkov SF, Demidov VE, Kalinikos BA, Srinivasan G, Slavin AN, Mantese JV (2006) Ferrite-ferroelectric layered structures for electrically and magnetically tunable microwave resonators. Appl Phys Lett 88:033503
3. Nan CW, Bichurin MI, Dong SX, Viehland D, Srinivasan G (2008) Multiferroic magnetoelectric composites: historical perspective, status, and future directions. J Appl Phys 103:031101
4. Murugavel P, Singh MP, Prellier W, Mercey B, Simon C, Raveau JB (2005) The role of ferroelectric-ferromagnetic layers on the properties of superlattice-based multiferroics. Appl Phys 97:103914
5. Chang KS, Aronova MA, Lin CL, Murakami M, Yu MH, Hattrick SJ, Famodu OO, Lee SY, Ramesh R, Wuttig M, Takeuchi I (2004) Exploration of artificial multiferroic thin-film heterostructures using composition spreads. Appl Phys Lett 84:3091–3093
6. Xie SH, Li JY, Liu YY, Lan LN, Jin G, Zhou YC (2008) Electrospinning and multiferroic properties of $NiFe_2O_4$–$Pb(Zr_{0.52}Ti_{0.48})O_3$ composite nanofibers. J Appl Phys 104:024115
7. Zhu J, Zhou LX, Huang W, Li YQ, Li YR (2009) Study on the growth and interfacial strain of $CoFe_2O_4/BaTiO_3$ bilayer films. J Cryst Growth 311:3300–3304
8. Zhang CL, Chen WQ, Xie SH, Yang JS, Li JY (2009) The magnetoelectric effects in multiferroic composite nanofibers. Appl Phys Lett 94:102907
9. Hua Z, Yang P, Huang H (2008) Sol-gel template synthesis and characterization of magnetoelectric $CoFe_2O_4/Pb(Zr_{0.52}Ti_{0.48})O_3$ nanotubes. Mater Chem Phys 107:541–546
10. Xie SH, Li JY, Qiao Y, Liu YY, Lan LN, Zhou YC, Tan ST (2003) Multiferroic $CoFe_2O_4$–$Pb(Zr_{0.52}Ti_{0.48})O_3$ nanofibers by electrospinning. Appl Phys Lett 92:062901
11. Shen XQ, Cao K, Zhou JX (2006) Preparation of ferromagnetic binary alloy fine fibers by organic gel-thermal reduction process. Trans Nonferrous Met Soc China 16:1003–1008
12. Xiang J, Shen XQ, Meng XF (2009) Preparation of Co-substituted MnZn ferrite fibers and their magnetic properties. Mater Chem Phys 114:362–366
13. Zhang CY, Shen XQ, Zhou JX, Jing MX, Cao K (2007) Preparation of spinel ferrite $NiFe_2O_4$ fibres by organic gel-thermal decomposition process. J Sol-Gel Sci Technol 42:95
14. Nakamoto K, Huang D, Wang RQ (1986) Infrared and Raman Spectra of Inorganic and Coordination Compounds[M]. The Press Co of Chemical Industry, Beijing, pp 231–244
15. Yu PF, Cui B, Shi QZ (2008) Preparation and characterization of $BaTiO_3$ powders and ceramics by sol-gel process using oleic acid as surfactant. Mater Sci Eng A 473:34–41
16. Zhang SP, Dong DW, Sui Y (2006) Preparation of core shell particles consisting of cobalt ferrite and silica by sol-gel process. J Alloys Compd 415:257–260
17. Wang LQ, Liu L, Xue DF (2007) Wet routes of high purity $BaTiO_3$ nanopowders. J Alloys Compd 440:78–83
18. Liu XM, Fu SY, Xiao HM, Huang CJ (2005) Synthesis of nanocrystalline spinel $CoFe_2O_4$ via a polymer-pyrolysis route. Phys B 370:14–21
19. Shobana MK, Rajendran V, Jeyasubramanian K, Suresh KN (2007) Preparation and characterisation of NiCo ferrite nanoparticles. Mater Lett 61:2616–2619
20. Shobana MK, Sankar S (2009) Synthesis and characterization of $Ni_{1-x}Co_xFe_2O_4$ nanoparticles. J Magn Magn Mater 321:3132–3137
21. Ramajo L, Castro MS, Reboredo MM (2007) Effect of silane as coupling agent on the dielectric properties of $BaTiO_3$-epoxy composites. Compos Part A Appl Sci Manuf 32:1852–1859
22. Yue Z, Zhou J, Li L, Zhang H, Gui Z (2000) Sythesis of nanocrystalline NiCuZn ferrite powders by sol-gel auto-combustion method. J Magn Magn Mater 208:55–60
23. Wu KH, Yu CH, Chang YC, Horng DN (2004) Effect of pH on the formation and combustion process of sol-gel auto-combustion derived NiZn ferrite/SiO_2 composites. J Solid State Chem 177:4119–4125
24. Peng CH, Hwang CC, Wan J, Tsai JS, Chen SY (2005) Microwave-absorbing characteristics for the composites of thermal-plastic polyurethane (TPU)-bonded NiZn-ferrites prepared by combustion synthesis method. Mater Sci Eng B 1(117):27–36
25. Chiu WS, Radiman S, Abd-Shukor R, Abdullah MH, Khiew PS (2008) Tunable coercivity of $CoFe_2O_4$ nanoparticles via thermal annealing treatment. J Alloys Compd 459:291–297
26. Stoner EC, Wohlfarth EPA (1991) Mechanism of magnetic hysteresis in heterogeneous alloys. IEEE Trans on Magn 27(4):3475–3518

27. Maaz K, Mumtaz A, Hasanain SK, Ceylan A (2007) Synthesis and magnetic properties of cobalt ferrite ($CoFe_2O_4$) nanoparticles prepared by wet chemical route. J Magn Magn Mater 308(2):289
28. Rashada MM, Mohamed RM, El-Shall H (2008) Magnetic properties of nanocrystalline Sm-substituted $CoFe_2O_4$ synthesized by citrate precursor method. J Mater Process Technol 198(1–3):139
29. Cheng Y, Zheng YH, Wang YS, Bao F, Qin Y (2005) Synthesis and magnetic properties of nickel ferrite nano-octahedra. J Solid State Chem 178(7):2394–2397
30. Singhal S, Singh J, Barthwal SK, Chandra K (2005) Preparation and characterization of nanosize nickel-substituted cobalt ferrites ($Co_{1-x}Ni_xFe_2O_4$). J Solid State Chem 178:3183–3189